Available online at www.sciencedirect.com
SCIENCE DIRECT®
Journal of Sound and Vibration 269 (2004) 3–17
JOURNAL OF SOUND AND VIBRATION
www.elsevier.com/locate/jsvi

Robust vibration control based on identified models

Jing Yuan*

Department of Mechanical Engineering, The Hong Kong Polytechnic University, Hunghom, Kowloon, Hong Kong

Received 17 July 2002; accepted 10 December 2002

Abstract

In active vibration control, model accuracy of a vibration field is crucial to the stability and performance of closed-loop systems, especially multiple-input–multiple-output feedback control systems. A state-space model is popular for the design of vibration controllers. Its accuracy may be affected by mode truncation, errors in eigenfunctions for a modal model or errors in mass/stiffness coefficients of finite elements for a finite element model. There are few analytical results on controller stability margins with respect to these errors. This paper proposes a controller based on transfer matrices identified from the measurement data, on the ground that the accuracy of transfer matrices is manageable by identification algorithms. The proposed controller is able to introduce active damping to vibration fields. An analytical link is available between the stability margin and identification errors for the proposed controller. These are important features analyzed theoretically and verified numerically and experimentally here.

1. Introduction

Feedback control is an important vibration control strategy. Many feedback vibration controllers are based on modal state feedback [1–4]. These schemes require accurate modal parameters such as eigenfunctions to design the controllers and obtain online modal feedback. The accuracy of eigenfunctions affects not only parameters of the controller but also the feedback state vector with which the actuation signal is synthesized.

A practical problem with modal controllers is the availability of eigenfunctions for vibration fields with irregular shapes or uncertain boundary conditions. In many applications, eigenfunctions are not available analytically and must be estimated with inevitable errors. For structures mounted with piezoelectric patches, the existence of eigenfunctions could be a problem [5]. This reason prompts the use of physical state feedback with multiple spring–mass [6,7] or finite element

*Tel.: +852-2766-7822; fax: +852-2365-4703.
E-mail address: mmjyuan@polyu.edu.hk (J. Yuan).

0022-460X/03/$ - see front matter
doi:10.1016/S0022-460X(02)01603-6

models [8–11] to avoid the eignfunctions. The physical state-space controllers still depend on accurate parameters such as mass/stiffness coefficients of finite elements. As common sense, a control engineer should not expect a model to match a real system exactly since it contains errors and uncertainties that affect the closed loop via a feedback controller. A problem with available vibration controllers is how to relate the stability margins analytically to inevitable errors in eigenfunctions or errors in mass/stiffness coefficients of finite elements.

An alternative model of a vibration field is the transfer function model (TFM) that represents paths from actuators to sensors in a vibration field. There are many mature algorithms for identification of transfer functions. The accuracy of these algorithms is sufficient to guarantee stable closed-loop systems in many applications [12]. For vibration control, an analytical link will be shown between the stability margin and identification errors for controllers based on TFMs. Such an analytical link fits the controller design problem into the framework of robust control theory. It is therefore natural for one to examine the possibility of designing vibration controllers based on TFMs identified from vibration fields.

The equivalence between TFM and other models prompts the proposal of a robust pole-placement controller on basis of the TFM. The controller will damp the entire vibration field, a feature to be analyzed theoretically and verified numerically and experimentally in this study. In view of model similarity between vibration and noise fields, the new method is also applicable to multiple-input–multiple-output (MIMO) active damping of enclosed noise fields.

Since a TFM is identified from actuation and sensor signals, it includes actuator and sensor dynamics. This study will analyze the differences between the TFM and the truncated state-space models with respect to actuator and sensor dynamics. It will be shown that a TFM provides a reasonably accurate and realistic way to establish closed-loop stability of a control system by taking actuator and sensor dynamics into analytical account. Details of theoretical analysis and numerical verification are presented in the following sections.

2. Mathematical model

The dynamics of a vibration or noise field, subject to the excitation of k_a actuators, can be described by a general second order equation

$$(\boldsymbol{M}s^2 + \boldsymbol{D}s + \boldsymbol{K})\boldsymbol{x} = \boldsymbol{B}\boldsymbol{f} + \boldsymbol{d} \quad \text{or} \quad \boldsymbol{A}(s)\boldsymbol{x} = \boldsymbol{B}\boldsymbol{f} + \boldsymbol{d}, \tag{1a}$$

where $\boldsymbol{M}$, $\boldsymbol{D}$, $\boldsymbol{K} \in \mathbf{R}^{m\times m}$ are the mass, viscosity damping, and stiffness matrices; $\boldsymbol{x} \in \mathbf{R}^m$ is the state vector; $\boldsymbol{B} \in \mathbf{R}^{m\times k_a}$ represents the actuator location matrix; $\boldsymbol{d} \in \mathbf{R}^m$ the disturbance vector and $\boldsymbol{f} \in \mathbf{R}^{k_a}$ the actuation force vector. The feedback signals are measured by k_s sensors such that

$$\boldsymbol{y} = \boldsymbol{C}\boldsymbol{x}, \tag{1b}$$

where $\boldsymbol{C} \in \mathbf{R}^{k_s\times m}$ is the sensor location matrix. The feed-through matrix is absent because its inclusion only increases the complexity of derivations without affecting the analytical results of this study.

The equation is expressed in the Laplace transform domain. It may be derived by different approaches, such as the finite element method, multiple spring–mass modelling, Rayleigh–Ritz

approximation or modal analysis with a proper truncation. Parameters of Eqs. (1a) and (1b) are assumed *not available*.

2.1. Mode truncation and actuator/sensor dynamics

For a modal state-space model, the transfer function from actuator location x_a to sensor location x_s is given by

$$H^*_{as}(s) = \sum_{i=1}^{\infty} \frac{\phi_i(x_s)\phi_i(x_a)}{s^2 + 2\xi_i\omega_i s + \omega_i^2},$$

where ξ_i is the damping ratio, ω_i the resonant frequency and $\phi_i(x)$ the eigenfunction of the ith vibration mode. The truncated version of this transfer function may be derived from Eq. (1a) as

$$H_{as}(s) = \sum_{i=1}^{m} \frac{\phi_i(x_s)\phi_i(x_a)}{s^2 + 2\xi_i\omega_i s + \omega_i^2} = \boldsymbol{c}_s \boldsymbol{A}^{-1}(s)\boldsymbol{b}_a. \tag{2a}$$

This approach is customarily adopted by many researchers in vibration research [1,3], where $\boldsymbol{c}_s$ is a row of matrix $\boldsymbol{C}$ and $\boldsymbol{b}_a$ is a column of matrix $\boldsymbol{B}$, with $\phi_i(x_s)$ and $\phi_i(x_a)$ as the respective elements. The least-square modal filter $\boldsymbol{x} = [\boldsymbol{C}^{\mathrm{T}}\boldsymbol{C}]^{-1}\boldsymbol{C}^{\mathrm{T}}\boldsymbol{y}$ is a popular tool to recover $\boldsymbol{x}$ from $\boldsymbol{y}$. Since rank $(\boldsymbol{C})$ is at most $\min\{m, k_s\}$, $\boldsymbol{x} = [\boldsymbol{C}^{\mathrm{T}}\boldsymbol{C}]^{-1}\boldsymbol{C}^{\mathrm{T}}\boldsymbol{y}$ is solvable only if $m \leqslant k_s$. The feedback vector $\boldsymbol{x}$ may be contaminated by parameter errors in $\boldsymbol{C}$. Other state-space controllers use $\boldsymbol{y}$ as the physical state vector [6–8], which means $\boldsymbol{y} = \boldsymbol{x}$ and $m = k_s$.

For the TFM approach, on the other hand, the same transfer function is given by

$$T^*_{as}(s) = \left[\sum_{i=1}^{\infty} \frac{\phi_i(x_a)\phi_i(x_s)}{s^2 + 2\xi_i\omega_i s + \omega_i^2}\right] F_a(s)F_s(s),$$

where $F_a(s)$ and $F_s(s)$ denote the actuator and sensor dynamics, respectively. The truncated TFM is given by

$$T_{as}(s) = \left[\sum_{i=1}^{m} \frac{\phi_i(x_a)\phi_i(x_s)}{s^2 + 2\xi_i\omega_i s + \omega_i^2}\right] F_a(s)F_s(s), \tag{2b}$$

where m is determined by the bandwidth of $F_a(s)$ and $F_s(s)$ but independent of k_s. The difference between a modal state-space model and a TFM, with respect to mode truncation and actuator/sensor dynamics, is clear by comparing Eqs. (2a) and (2b). Obviously, Eq. (2b) is not a straightforward solution of Eq. (1a) as Eq. (2a).

Consider, for example, a simplified case with a first order actuator/sensor dynamics $F_a(s)F_s(s) = 1/s + \sigma$. Its substitution into Eq. (2b) leads to a partial fraction expansion

$$T_{as}(s) = \frac{k_\sigma}{s + \sigma} - \sum_{i=1}^{m} \frac{\phi_i(x_a)\phi_i(x_s)}{\omega_i^2 + \sigma^2 - 2\xi_i\omega_i\sigma} \frac{s + 2\xi_i\omega_i - \sigma}{s^2 + 2\xi_i\omega_i s + \omega_i^2}, \tag{2c}$$

where

$$k_\sigma = \sum_{i=1}^{m} \frac{\phi_i(x_a)\phi_i(x_s)}{\omega_i^2 + \sigma^2 - 2\xi_i\omega_i\sigma}.$$

$T_{as}(s)$ is more accurate than $H_{as}(s)$ since $F_a(s)$ and $F_s(s)$ cause phase and magnitude distortions to all modes, as shown in Eq. (2c). The inclusion of $F_a(s)$ and $F_s(s)$ implies an analytical impact of actuator/sensor dynamics to a state-space model in terms of elements of $\boldsymbol{A}(s)$, $\boldsymbol{B}$ and $\boldsymbol{C}$. Such an analytical treatment has not been seen in the stability analysis of vibration controllers based on state-space models.

2.2. Identification of transfer functions

In practice, eigenfunctions and actuator/sensor dynamic models may not be available accurately. It is always possible to identify these models from experimental data. Almost all identification results are based on input excitations and output measurements that inevitably involve actuators and sensors. A control system generates a signal u_t and feeds it to an actuator to excite the vibration field. A vibration signal y_t is measured and sampled into a computer as v_t after filtered by an anti-alias filter.

The signal sequences u_t and v_t may be used to identify a discrete-time single-input–single-output (SISO) transfer function $T_{as}(z) = n(z)/d(z)$ with actuator/sensor dynamics hidden in $d(z) = z^{2m} + \sum_{I=1}^{2M} d_i z^{2m-i}$ and $n(z) = \sum_{i=1}^{2m} n_i z^{2m-i}$. Parameters of $d(z)$ and $n(z)$ are identified via an autoregressive moving-average (ARMA) expression

$$v_t + \hat{d}_1 v_{t-1} + \cdots + \hat{d}_{2m} v_{t-2m} - \hat{n}_1 u_{t-1} - \cdots - \hat{n}_{2m} u_{t-2m} = \varepsilon_t, \tag{3}$$

where ε_t is the residual error.

Alternatively, one may apply the above process to identify the actuator/sensor transfer functions and plant transfer functions separately and include the actuator/sensor dynamics in the controller model. Practically, it is more convenient to identify a single transfer function $T_{as}(z)$ that includes all unknown dynamic effects. Since u_t has to pass an actuator before it can excite the vibration field and a vibration signal is available as a sensor signal v_t, it is actually difficult and unnecessary to separate the actuator/sensor dynamics explicitly from $T_{as}(z)$.

The identification errors are analytically described by $\Delta d(z) = d(z) - \hat{d}(z)$ and $\Delta n(z) = n(z) - \hat{n}(z)$ in the form of $\Delta d(z) v_t - \Delta n(z) u_t = \varepsilon_t$ [12]. Many identification algorithms are analyzed in Ref. [12] that drive ε_t to zero. If u_t is persistently exciting the vibration field, then $||\Delta d(z)||$ and $||\Delta n(z)||$ converge to zero as well. In practice, due to mode truncation, the algorithms described in Ref. [12] will drive $|\varepsilon_t|$, $||\Delta d(z)||$, and $||\Delta n(z)||$ to be smaller or equal to prescribed bounds under persistent excitation.

For MIMO application, a transfer matrix is a combination of scalar transfer functions. Each of them can be identified with an estimation error bounded by small bounds. Solving $\boldsymbol{y}$ from Eqs. (1a) and (1b), one obtains $\boldsymbol{y} = \mathrm{C}\boldsymbol{A}^{-1}(s)(\boldsymbol{B}\boldsymbol{f} + \boldsymbol{d})$. The actuation forces are generated by actuator filters $\boldsymbol{f} = \boldsymbol{F}_a(s)\boldsymbol{u}$ where $\boldsymbol{u}$ is the control signal and $\boldsymbol{F}_a(s)$ is a diagonal transfer matrix. The vibration signals are measured by sensor filters as $\boldsymbol{v} = \boldsymbol{F}_s(s)\boldsymbol{y}$ where $\boldsymbol{v}$ is available to the controller and subject to the distortion of diagonal filter transfer matrix $\boldsymbol{F}_s(s)$. This implies

$$\boldsymbol{v} = \boldsymbol{L}(s)\boldsymbol{A}^{-1}(s)\boldsymbol{H}(s)\boldsymbol{u} + \boldsymbol{\eta} = \boldsymbol{T}(s)\boldsymbol{u} + \boldsymbol{\eta}, \tag{4}$$

where $\boldsymbol{T}(s) = \boldsymbol{L}(s)\boldsymbol{A}^{-1}(s)\boldsymbol{H}(s)$ is a MIMO transfer matrix;

$$\boldsymbol{H}(s) = \boldsymbol{B}\boldsymbol{F}a(s), \quad \boldsymbol{L}(s) = \boldsymbol{F}_s(s)\boldsymbol{C} \quad \text{and} \quad \boldsymbol{\eta} = \boldsymbol{L}(s)\boldsymbol{A}^{-1}(s)\boldsymbol{d}. \tag{5}$$

The discrete-time version of $\boldsymbol{T}(s)$ is denoted by $\boldsymbol{T}(z)$. In the next subsection, the continuous-time model $\boldsymbol{T}(s)$ serves as the basis to show active damping effects of the proposed controller. Thereafter, the discrete-time model $\boldsymbol{T}(z)$ will be the basis of design and stability analysis for the proposed vibration controller.

2.3. Active damping by the proposed controller

There are two objectives for vibration control. One is the creation of local quiet zones by minimizing sensed signals; the other is active damping by modifying closed-loop eigenvalues. A controller designed for one objective is not necessarily suitable for the other. Since a TFM includes more modes than sensors ($m > k_s$) and these modes are subject to the distortion of actuator/sensor filters, sensor signals $\boldsymbol{v}$ contain partial and distorted information about $\boldsymbol{x}$. Minimization of $\boldsymbol{v}$ does not necessarily minimize $\boldsymbol{x}$. The pole-placement controller $\boldsymbol{G}(s)$ is more suitable for active damping. A substitution of $\boldsymbol{u} = -\boldsymbol{G}(s)\boldsymbol{v}$ into Eq. (4) leads to

$$\boldsymbol{v} = [\boldsymbol{I} + \boldsymbol{T}(s)\boldsymbol{G}(s)]^{-1}\boldsymbol{\eta} = [\boldsymbol{I} + \boldsymbol{L}(s)\boldsymbol{A}^{-1}(s)\boldsymbol{H}(s)\boldsymbol{G}(s)]^{-1}\boldsymbol{\eta}, \tag{6}$$

for the TFM closed loop.

In view of actuator/sensor dynamics, one should substitute $\boldsymbol{f} = -\boldsymbol{F}_a(s)\boldsymbol{G}(s)\boldsymbol{L}(s)\boldsymbol{x}$ in Eq. (1a) to derive the closed-loop solution for the state vector $\boldsymbol{x}$ as

$$\boldsymbol{x} = [\boldsymbol{A}(s) + \boldsymbol{H}(s)\boldsymbol{G}(s)\boldsymbol{L}(s)]^{-1}\boldsymbol{d}. \tag{7}$$

By some routine calculations, it is not difficult to verify the following identity:

$$[\boldsymbol{I} + \boldsymbol{L}(s)\boldsymbol{A}^{-1}(s)\boldsymbol{H}(s)\boldsymbol{G}(s)]\{\boldsymbol{I} - \boldsymbol{L}(s)[\boldsymbol{A}(s) + \boldsymbol{H}(s)\boldsymbol{G}(s)\boldsymbol{L}(s)]^{-1}\boldsymbol{H}(s)\boldsymbol{G}(s)\} = \boldsymbol{I}. \tag{8}$$

It becomes clear that Eq. (6) is equivalent to

$$\boldsymbol{v} = \{\boldsymbol{I} - \boldsymbol{L}(s)[\boldsymbol{A}(s) + \boldsymbol{H}(s)\boldsymbol{G}(s)\boldsymbol{L}(s)]^{-1}\boldsymbol{H}(s)\boldsymbol{G}(s)\}\boldsymbol{\eta}, \tag{9}$$

which involves the same inverse of $\boldsymbol{A}(s) + \boldsymbol{H}(s)\boldsymbol{G}(s)\boldsymbol{L}(s)$ as Eq. (7). Therefore, closed-loop poles of Eq. (6) are also closed-loop poles of Eq. (7). The objective of active damping is based on such equivalence.

In practice, a controller may be based on a discrete-time transfer matrix expressed as $\boldsymbol{T}(z) = \boldsymbol{D}_l^{-1}(z)\boldsymbol{N}_l(z) = \boldsymbol{N}_r(z)\boldsymbol{D}_r^{-1}(z)$ where $\boldsymbol{D}_l^{-1}(z)\boldsymbol{N}_l(z)$ and $\boldsymbol{N}_r(z)\boldsymbol{D}_r^{-1}(z)$ are, respectively, the left and right matrix fraction descriptions (MFDs) [13]. The left MFD has an ARMA expression $\boldsymbol{D}_l(z)\boldsymbol{v}_t - \boldsymbol{N}_l(z)\boldsymbol{u}_t = \boldsymbol{\varepsilon}_t$ and is identifiable by any algorithm described in Ref. [12]. Similar to the SISO example of Eq. (3), identification errors of $\boldsymbol{T}(z)$ are denoted as $\Delta\boldsymbol{D}_l(z) = \boldsymbol{D}_l(z) - \hat{\boldsymbol{D}}_l(z)$ and $\Delta\boldsymbol{N}_l(z) = \boldsymbol{N}_l(z) - \hat{\boldsymbol{N}}_l(z)$, respectively. Convergence of $||\Delta\boldsymbol{D}_l(z)||_\infty$ and $||\Delta\boldsymbol{N}_l(z)||_\infty$ to be smaller than or equal to prescribed small bounds are possible under persistent excitation [12]. If the magnitude of disturbance is bounded by a small value, then an adaptive pole-placement controller is available in Ref. [13] with guaranteed closed-loop stability when the controller is based on an online TFM. In vibrations systems, disturbance $\boldsymbol{d}$ may exceed the tolerances of adaptive controllers. It is easier to obtain offline estimates $\hat{\boldsymbol{D}}_l(z) \in \mathbf{C}^{k_s \times k_s}$ and $\hat{\boldsymbol{N}}_l(z) \in \mathbf{C}^{k_a \times k_s}$ with reasonably small errors $||\Delta\boldsymbol{D}_l(z)||_\infty \leqslant \delta_{dl}$ and $||\Delta\boldsymbol{N}_l(z)||_\infty \leqslant \delta_{nl}$ by shutting off $\boldsymbol{d}$. The right MFD of $\boldsymbol{T}(z)$ can be obtained from its left MFD as $\hat{\boldsymbol{D}}_r(z) \in \mathbf{C}^{k_a \times k_a}$ and $\hat{\boldsymbol{N}}_r(z) \in \mathbf{C}^{k_a \times k_s}$ with small errors $||\Delta\boldsymbol{D}_r(z)||_\infty \leqslant \delta_{dr}$ and $||\Delta\boldsymbol{N}_r(z)||_\infty \leqslant \delta_{nr}$. These are the analytical design basis for the proposed controller.

3. Controller design and analysis

In the previous section, the closed-loop eigenvalues of the state-space model Eq. (1a) are shown equivalent to the eigenvalues of $\boldsymbol{I} + \boldsymbol{T}(s)\boldsymbol{G}(s)$. The focus of this section is to design a digital controller $\boldsymbol{G}(z)$ such that roots of $\det[\boldsymbol{I} + \boldsymbol{T}(z)\boldsymbol{G}(z)] = 0$ be placed in prescribed locations in the complex plane.

3.1. Controller structure

There are generally two types of pole-placement controllers. A static one requires full state feedback to place all poles, though it is able to place partial poles with output feedback. A dynamic pole-placement controller, on the other hand, is able to place all poles with output feedback. It is more suitable for the purpose of this study. The controller has a discrete-time transfer matrix in the form of left MFD

$$\boldsymbol{G}(z) = \boldsymbol{Q}_l^{-1}(z)\boldsymbol{R}_l(z), \tag{10}$$

where $\boldsymbol{Q}_l(s) = \boldsymbol{Q}_0 + \boldsymbol{Q}_1 z^{-1} + \cdots + \boldsymbol{Q}_{k-1} z^{-k-1}$ and $\boldsymbol{R}_l(s) = \boldsymbol{R}_0 + \boldsymbol{R}_1 z^{-1} + \cdots + \boldsymbol{R}_{k+r-1} z^{-k-r+1}$ are $k_a \times k_a$ and $k_a \times k_s$ polynomial matrices, respectively; the order of the controller is related to k, which may be the smallest positive integer such that

$$k \geqslant n\frac{k_a}{k_s} - r. \tag{11}$$

Using Eq. (10) and the right MFD of $\boldsymbol{T}(z)$, one obtains $\boldsymbol{I} + \boldsymbol{T}(z)\boldsymbol{G}(z) = \boldsymbol{I} + \boldsymbol{N}_r(z)\boldsymbol{D}_r^{-1}(z)\boldsymbol{Q}_l^{-1}(z)\boldsymbol{R}_l(z)$. It is not difficult to verify equality

$$\boldsymbol{I} = \{\boldsymbol{I} + \boldsymbol{N}_r(z)\boldsymbol{D}_r^{-1}(z)\boldsymbol{Q}_l^{-1}(z)\boldsymbol{R}_l(z)\}\{\boldsymbol{I} - \boldsymbol{N}_r(z)[\boldsymbol{Q}_l(z)\boldsymbol{D}_r(z) + \boldsymbol{R}_l(z)\boldsymbol{N}_r(z)]^{-1}\boldsymbol{R}_l(z)\} \tag{12}$$

by some routine calculations. It turns out that the discrete-time version of Eq. (6) is equivalent to

$$\boldsymbol{v} = [\boldsymbol{I} + \boldsymbol{T}(z)\boldsymbol{G}(z)]^{-1}\boldsymbol{\eta} = \{\boldsymbol{I} - \boldsymbol{N}_r(z)[\boldsymbol{Q}_l(z)\boldsymbol{D}_r(z) + \boldsymbol{R}_l(z)\boldsymbol{N}_r(z)]^{-1}\boldsymbol{R}_l(z)\}\boldsymbol{\eta}, \tag{13}$$

which involves the inverse of $\boldsymbol{Q}_l(z)\boldsymbol{D}_r(z) + \boldsymbol{R}_l(z)\boldsymbol{N}_r(z)$ with a dimension $k_a \times k_a$. Since most active vibration controllers use fewer actuators than feedback sensors ($k_a < k_s$), the use of Eq. (13) helps to reduce the complexity of controller design. If $k_a > k_s$ instead, then one should use the left MFD of $\boldsymbol{T}(z)$ and work on an equivalent $k_s \times k_s$ matrix. Starting from this step, the focus will be the roots of $\det[\boldsymbol{Q}_l(z)\boldsymbol{D}_r(z) + \boldsymbol{R}_l(z)\boldsymbol{N}_r(z)] = 0$ since these are closed-loop eigenvalues of the vibration field.

3.2. Solution of controller parameters

The closed-loop poles can be placed by means of a $k_a \times k_a$ prototype polynomial matrix $\boldsymbol{P}(z) = \boldsymbol{P}_0 + \boldsymbol{P}_1 z^{-1} + \cdots + \boldsymbol{P}_{n+k-1} z^{-n-k+1} + \boldsymbol{P}_{n+k} z^{-n-k}$ with degree $n + k$. There are many ways to prescribe matrices $\boldsymbol{P}_i\, 0 \leqslant i \leqslant (n + k)$ such that roots of $\det[\boldsymbol{P}(z)] = 0$ are in given locations in the complex plane. One possible way is to construct $\boldsymbol{P}(z) = \prod(\boldsymbol{I}_a + \boldsymbol{\Lambda}_i z^{-1})$ with $k_a \times k_a$ matrices $\boldsymbol{I}_a$ and $\boldsymbol{\Lambda}_i$. Here $\boldsymbol{I}_a$ is an identity and $\boldsymbol{\Lambda}_i$ is freely selected by a control engineer to represent k_a given poles. The most straightforward way is to let $\boldsymbol{\Lambda}_i$ be a diagonal matrix whose diagonal elements are k_a real poles. It is also possible to construct $\boldsymbol{P}(z)$ via matrices like $(\boldsymbol{I}_a + \boldsymbol{\Xi}_i z^{-1} + \boldsymbol{\Lambda}_i z^{-2})$ that

represents given complex poles with real matrices $\boldsymbol{\Xi}_i$ and $\boldsymbol{\Lambda}_i$. The objective of the controller is to match $\boldsymbol{Q}_l(z)\boldsymbol{D}_r(z) + \boldsymbol{R}_l(z)\boldsymbol{N}_r(z) = \boldsymbol{P}^{\mathrm{T}}(z)$, whose transpose is a Bezout equation

$$\boldsymbol{P}(z) = \boldsymbol{D}_r^{\mathrm{T}}(z)\boldsymbol{Q}_l^{\mathrm{T}}(z) + \boldsymbol{N}_r^{\mathrm{T}}(z)\boldsymbol{R}_l^{\mathrm{T}}(z). \tag{14}$$

The Bezout equation is a mathematical tool frequently used in controller design [12,13]. With $\boldsymbol{Q}_l(z)$ and $\boldsymbol{R}_l(z)$ satisfying Eqs. (14) and (13) becomes

$$\boldsymbol{v} = [\boldsymbol{I} + \boldsymbol{T}(z)\boldsymbol{G}(z)]^{-1}\boldsymbol{\eta} = [\boldsymbol{I} - N_r(z)\boldsymbol{P}^{-\mathrm{T}}(z)\boldsymbol{R}_l(z)]\boldsymbol{\eta}. \tag{15}$$

As a result, closed-loop eigenvalues of the vibration field are placed by the controller to be roots of $\det[\boldsymbol{P}(z)] = 0$, due to the equivalence of Eqs. (6) and (7) and the equivalence of Eqs. (6), (13) and (15).

In summary, the objective of pole-placement is achievable by (a) a freely selectable prototype $\boldsymbol{P}(z)$ and (b) a controller whose left MFD numerator $\boldsymbol{R}_l(z)$ and denominators $\boldsymbol{Q}_l(z)$ satisfy Eq. (14) that has an alternative expression

$$\begin{bmatrix} \mathbf{P}_0 \\ \mathbf{P}_1 \\ \vdots \\ \mathbf{P}_{n+k-1} \\ \mathbf{P}_{n+k} \end{bmatrix} = \underbrace{\begin{bmatrix} \boldsymbol{D}_0^{\mathrm{T}} & \cdots & \boldsymbol{O}_a \\ \vdots & \ddots & \boldsymbol{O}_a \\ \boldsymbol{D}_n^{T} & \vdots & \boldsymbol{D}_0^{\mathrm{T}} \\ \boldsymbol{O}_a & \ddots & \vdots \\ \boldsymbol{O}_a & \cdots & \boldsymbol{D}_n^{\mathrm{T}} \end{bmatrix}}_{k\times k_a} \underbrace{\begin{bmatrix} \boldsymbol{N}_0^{\mathrm{T}} & \cdots & \boldsymbol{O}_{as} \\ \vdots & \ddots & \boldsymbol{O}_{as} \\ \boldsymbol{N}_{n-r}^{\mathrm{T}} & \vdots & \boldsymbol{N}_0^{\mathrm{T}} \\ \boldsymbol{O}_{as} & \ddots & \vdots \\ \boldsymbol{O}_{as} & \cdots & \boldsymbol{N}_{n-r}^{\mathrm{T}} \end{bmatrix}}_{(k+r)\times k_s} \begin{bmatrix} \boldsymbol{Q}_0^{\mathrm{T}} \\ \vdots \\ \boldsymbol{Q}_{k-1}^{\mathrm{T}} \\ \boldsymbol{R}_0^{\mathrm{T}} \\ \vdots \\ \boldsymbol{R}_{n+r-1}^{\mathrm{T}} \end{bmatrix}. \tag{16}$$

The $[(n+k)k_a] \times [kk_a + (k+r)k_s]$ matrix in Eq. (16) is known as the generalized Sylvester matrix (GSM) [13] where $\boldsymbol{O}_a$ is a $k_a \times k_a$ zero and $\boldsymbol{O}_{as}$ is a $k_a \times k_s$ zero matrix. The rank of the GSM must be $(n+k)k_a$ in order for Eq. (16) to be solvable. This is not a problem if $\boldsymbol{v}$ is controllable by $\boldsymbol{u}$ [13]. Since $\boldsymbol{T}(z)$ is identified from data sequences $\boldsymbol{u}$ and $\boldsymbol{v}$, the uncontrollable modes cannot be excited by $\boldsymbol{u}$ and the unobservable modes cannot be measured by $\boldsymbol{v}$. If $\boldsymbol{u}$ satisfies the condition of persistent excitation, $\boldsymbol{T}(z)$ will converge to a controllable transfer matrix by one of the identification algorithms described in Ref. [12].

Matrix $\boldsymbol{N}_0$ in Eq. (16) should be zero if the feed-through matrix of Eq. (1) is zero or if the TFM involves a propagation delay. Similar treatment applies to the cases when the delay is $l < n - r$ sample intervals. That means the substitution of a zero $\boldsymbol{N}_i$ for $0 \leqslant i \leqslant l$ in Eq. (16) without affecting the solvability of $\boldsymbol{Q}_l(z)$ and $\boldsymbol{R}_l(z)$. This design procedure is most suitable for $k_a = 1$ such that $\boldsymbol{Q}_l(z)$ reduces to a scalar polynomial. For $k_a > 1$, an alternative solution is to design $k_a - 1$ static controllers to place partial closed-loop poles. Each of these controllers can be designed properly so that it places closed-loop poles that are not controllable to the remaining actuators [14]. The last controller is a dynamic one to place the remaining poles.

In practice, a continuous-time TFM may be identified and converted to a right MFD $\boldsymbol{T}(s) = \boldsymbol{N}_r(s)\boldsymbol{D}_r^{-1}(s)$, where $\boldsymbol{D}_r(s) = \boldsymbol{D}_0 s^n + \boldsymbol{D}_1 s^{n-1} + \cdots + \boldsymbol{D}_n$ and $\boldsymbol{N}_r(s) = \boldsymbol{N}_1 s^{n-r} + \cdots + \boldsymbol{N}_{n-r}$ are expressed in the Laplace transform domain. Other polynomials in Eq. (16), such as $\boldsymbol{P}(s)$, $\boldsymbol{Q}_l(s)$ and $\boldsymbol{R}_l(s)$, should also be expressed in the Laplace transform, as shown in the simulation.

3.3. Stability margin and robustness

In reality, $\boldsymbol{D}_r(z)$ and $\boldsymbol{N}_r(z)$ are not available and their estimates are substituted instead. As a result, Eq. (14) becomes $\boldsymbol{P}(z) = \hat{\boldsymbol{D}}_r^{\mathrm{T}}(z)\boldsymbol{Q}_l^{\mathrm{T}}(z) + \hat{\boldsymbol{N}}_r^{\mathrm{T}}(z)\boldsymbol{R}_l^{\mathrm{T}}(z)$ for the solution of controller matrices $\boldsymbol{Q}_l(z)$ and $\boldsymbol{R}_l(z)$ from an identified TFM. The modified Bezout equation is equivalent to

$$\boldsymbol{P}(z) + \Delta\boldsymbol{D}_r^{\mathrm{T}}\boldsymbol{Q}_l^{\mathrm{T}}(z) + \Delta\boldsymbol{N}_r^{\mathrm{T}}\boldsymbol{R}_l^{\mathrm{T}}(z) = \boldsymbol{D}_r^{\mathrm{T}}(z)\boldsymbol{Q}_l^{\mathrm{T}}(z) + \boldsymbol{N}_r^{\mathrm{T}}(z)\boldsymbol{R}_l^{\mathrm{T}}(z), \tag{17}$$

upon substitution of $\hat{\boldsymbol{D}}_r = \boldsymbol{D}_r - \Delta\boldsymbol{D}_r$ and $\hat{\boldsymbol{N}}_r = \boldsymbol{N}_r - \Delta\boldsymbol{N}_r$. As a result, Eq. (13) becomes

$$\boldsymbol{v} = [\boldsymbol{I} + \boldsymbol{T}(z)\boldsymbol{G}(z)]^{-1}\boldsymbol{\eta} = \{\boldsymbol{I} - \boldsymbol{N}_r(z)[\boldsymbol{P}(z) + \Delta\boldsymbol{D}_r^{\mathrm{T}}\boldsymbol{Q}_l^{\mathrm{T}}(z) + \Delta\boldsymbol{N}_r^{\mathrm{T}}\boldsymbol{R}_l^{\mathrm{T}}(z)]^{-1}\boldsymbol{R}_l(z)\}\boldsymbol{\eta}, \tag{18}$$

when $\hat{\boldsymbol{D}}_r(z)$ and $\hat{\boldsymbol{N}}_r(z)$ are substituted to obtain the controller matrices $\boldsymbol{Q}_l(z)$ and $\boldsymbol{R}_l(z)$. The identification errors cause the closed-loop eigenvalues to be roots of

$$\det[\boldsymbol{P}(z) + \Delta\boldsymbol{D}_r^{\mathrm{T}}\boldsymbol{Q}_l^{\mathrm{T}}(z) + \Delta\boldsymbol{N}_r^{\mathrm{T}}\boldsymbol{R}_l^{\mathrm{T}}(z)] = 0, \tag{19}$$

or, equivalently, roots of

$$\det\{\boldsymbol{I} + [\Delta\boldsymbol{D}_r^{\mathrm{T}}\boldsymbol{Q}_l^{\mathrm{T}}(z) + \Delta\boldsymbol{N}_r^{\mathrm{T}}\boldsymbol{R}_l^{\mathrm{T}}(z)]\boldsymbol{P}^{-1}(z)\}\det[\boldsymbol{P}(z)] = 0. \tag{20}$$

The closed-loop system is stable if $||[\Delta\boldsymbol{D}_r^{\mathrm{T}}\boldsymbol{Q}_l^{\mathrm{T}}(z) + \Delta\boldsymbol{N}_r^{\mathrm{T}}\boldsymbol{R}_l^{\mathrm{T}}(z)]\boldsymbol{P}^{-1}(z)||_\infty < 1$ by applying the small gain theory to the above expression.

As explained in Section 2.3, identification errors of $\hat{\boldsymbol{D}}_r(z)$ and $\hat{\boldsymbol{N}}_r(z)$ are reasonably small $||\Delta\boldsymbol{D}_r(z)||_\infty \leqslant \delta_{dr}$ and $||\Delta\boldsymbol{N}_r(z)||_\infty \leqslant \delta_{nr}$ if one of the algorithms analyzed in Ref. [12] is used to identify $\boldsymbol{T}(z)$ in a persistently excited vibration system. Therefore, the stability margin is analytically related to the identification error bounds in an $\mathbf{H}_\infty$ constraint

$$\delta_{\mathrm{dr}}\left|\left|\boldsymbol{Q}_l^{\mathrm{T}}(z)\boldsymbol{P}^{-1}(z)\right|\right|_\infty + \delta_{nr}\left|\left|\boldsymbol{R}_l^{\mathrm{T}}(z)\boldsymbol{P}^{-1}(z)\right|\right|_\infty < 1. \tag{21}$$

Since the objective of the proposed controller is active damping of the vibration field, it is desirable to place the closed-loop eigenvalues of the vibration field in a disk with radius $\gamma < 1$. In order to achieve the objective, $\boldsymbol{P}(z)$ is no longer freely prescribed by a control engineer. Instead, it must satisfy (C1) roots of $\det[\boldsymbol{P}(z)] = 0$ are inside a disk with radius $\gamma < 1$; and (C2) $\delta_{\mathrm{dr}}||\boldsymbol{Q}_l^{\mathrm{T}}(z)\boldsymbol{P}^{-1}(z)||_\infty + \delta_{nr}||\boldsymbol{R}_l^{\mathrm{T}}(z)\boldsymbol{P}^{-1}(z)||_\infty < \gamma$.

These conditions fit well into the framework of the $\mathbf{H}_\infty$ control theory. The problem is solvable by the available numerical tools such as the Robust control toolbox or the LMI control toolbox of Matlab. This is an advantage of the TFM approach. For controllers based on the modal or physical state-space models, it is an open problem to find analytical links between stability margin and errors in the eigenfunctions or errors in the mass/stiffness coefficients of finite elements.

4. Numerical and experimental verification

A numerical example is presented here to demonstrate how active damping is possible by a controller based on the TFM. The vibration structure is a 1-D cantilever beam satisfying the Bernoulli–Euler equation.

4.1. Simulation conditions

With a unit length $L = 1$, the ith eigenvalue of the beam is denoted by λ_i as the ith root of $\cos(\lambda_i)\cosh(\lambda_i) + 1 = 0$. The ith resonant frequency may be calculated by $\omega_i = (\lambda_i)^2\sqrt{EI/\rho}$ where ρ is the mass density; E is Young's modulus of elasticity and I the moment of inertia of the cross-sectional area with respect to the neutral axis. Theoretically the proposed controller is able to damp as many modes as the actuator and feedback sensor can excite and observe. Practically, active control devices are applied to the low frequency ranges since high order modes are absorbed more effectively by inexpensive passive methods. For this reason, the model only includes $m = 5$ modes with resonant frequencies $\omega_1 = 0.70\,\text{rad/s}$, $\omega_2 = 4.41\,\text{rad/s}$, $\omega_3 = 12.34\,\text{rad/s}$, $\omega_4 = 24.18\,\text{rad/s}$ and $\omega_5 = 39.97\,\text{rad/s}$ by assuming $\sqrt{EI/\rho} = 0.2$. The eigenfunctions are analytically available as [15]

$$\varphi_i(x) = [\cosh(\lambda_i x) - \cos(\lambda_i x)] - \mu_i[\sinh(\lambda_i x) - \sin(\lambda_i x)],$$

where

$$\mu_i = \frac{\cos(\lambda_i) + \cosh(\lambda_i)}{\sin(\lambda_i) + \sinh(\lambda_i)}.$$

If fitted into Eq. (1a), these parameters make $\boldsymbol{K}$ diagonal, $\boldsymbol{M}$ identity and $\det(\mathbf{M}s^2 + \mathbf{K}) = \prod_{k=1}^{5}(s^2 + \omega_k^2)$. Elements of $\boldsymbol{B}$ and $\boldsymbol{C}$ are eigenfunctions sampled at the actuator and sensor locations, respectively.

It is assumed that $k_a = 1$ actuator and $k_s = 3$ sensors are mounded on the beam at $x_a = 0.58$, $\boldsymbol{x}_s = [0.38, 0.58, 0.88]^{\mathrm{T}}$ as shown in Fig. 1 by an arrow and three thick dots. The actuation force is assumed to be a point force. A (point force) disturbance is assumed to act on $x_d = 0.68$ to inject a white noise. In order to examine the damping effect, four monitor sensors are placed at $\boldsymbol{x}_m = [0.28, 0.48, 0.78, 0.98]^{\mathrm{T}}$ as shown in Fig. 1 by circles. These sensors are independent of the control loop because their signals are not accessible by the controller.

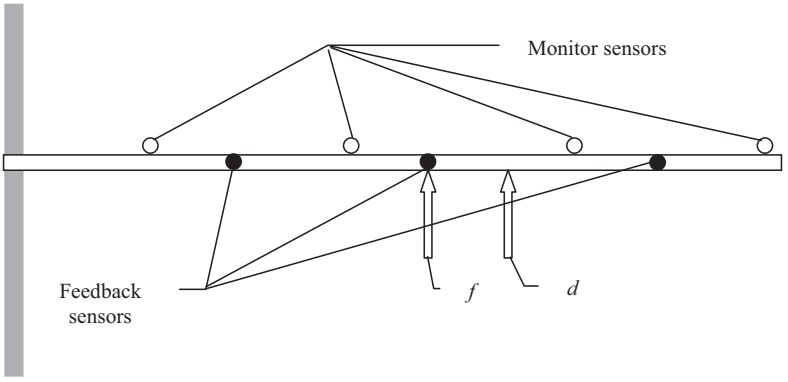

Fig. 1. Actuator, sensor and disturbance locations on a cantilever beam.

4.2. Case 1: damping five modes

For the numerical example, the TFM is a 3×1 polynomial matrix $\boldsymbol{T}(s) = \boldsymbol{N}^{\mathrm{T}}(s)d^{-1}(s)$ where $d(s)$ is a scalar polynomial and $\boldsymbol{N}(s)$ is a 1×3 polynomial matrix with degrees $n = 10$ and $n - r = 8$, respectively, when ideal actuator/sensors are assumed. For $m = 5 > k_s = 3 > k_a = 1$, the inverse matrices in Eqs. (6), (7) and (13) are 3×3 ($k_s \times k_s$), 5×5 ($m \times m$) and 1×1 ($k_a \times k_a$), respectively. Since these models are equivalent, the easiest way to assign closed-loop poles is to work with Eq. (13). In case $k_a > k_s$, one should work with Eq. (6) by using the left MFD of $\boldsymbol{T}(s)$ as explained in the previous section. In any case, m is larger than either k_s or k_a when actuator/sensor dynamics are included.

The proposed controller has a transfer matrix $\boldsymbol{G}(s) = q^{-1}(s)\boldsymbol{R}^{\mathrm{T}}(s)$ where $q(s)$ is a scalar polynomial and $\boldsymbol{R}(s)$ is a 3×1 polynomial matrix. The order of the controller is $k = 2$ as determined by Eq. (11) for this example. Coefficients of $q(s)$ and $\boldsymbol{R}(s)$ are solved by Eq. (16). A prototype polynomial $p(s) = (s + 12)\prod_{k=1}^{5}(s^2 + 0.16\omega_k s + \omega_k^2)$ is used to prescribe closed-loop poles that are also closed-loop eigenvalues of the beam. The vibration spectra are plotted in Figs. 2–5 as gray solid lines against the uncontrolled vibration spectra in back dash–dot lines. These are signals independent and not accessible to the controller. The damping effects are therefore to the entire vibration field.

In this test, attempts have been made to place poles with higher damping ratios. The controller is able to place the corresponding poles. The resonant peaks are damped at the expense of enhancing vibration spectra in other frequency ranges. Spectra plotted in Figs. 2–5 by gray lines form a set of trade-off results between damping ratio and controller gains. One of the reasons

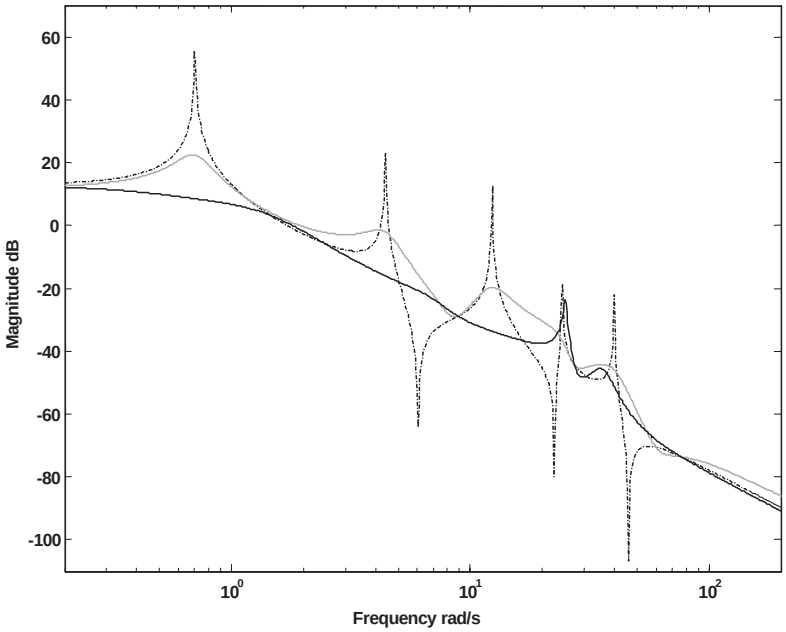

Fig. 2. Vibration spectra measured at $x_m = 0.98$, with the dash-dot line for uncontrolled case; the gray solid line for case 1 and the black solid line for case 2.

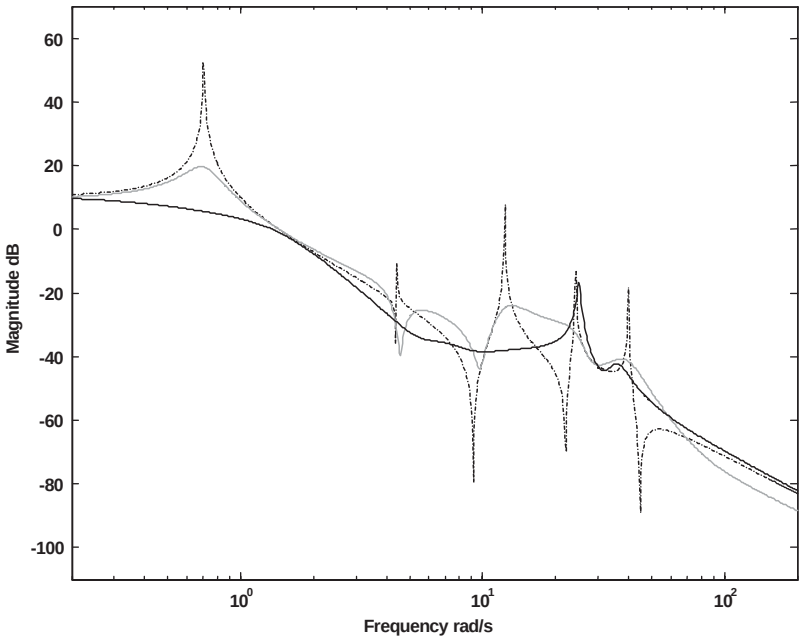

Fig. 3. Vibration spectra measured at $x_m = 0.78$, with the dash-dot line for uncontrolled case; the gray solid line for case 1 and the black solid line for case 2.

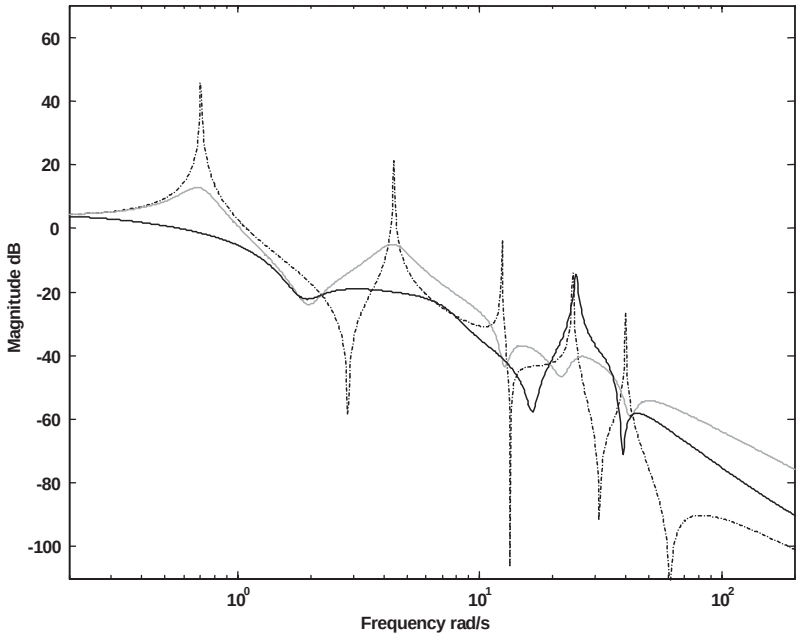

Fig. 4. Vibration spectra measured at $x_m = 0.48$, with the dash-dot line for uncontrolled case; the gray solid line for case 1 and the black solid line for case 2.

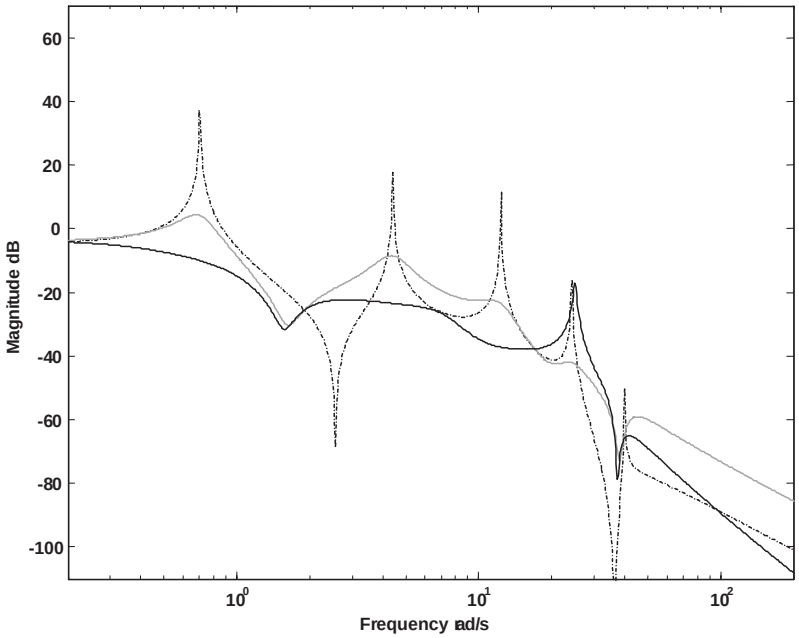

Fig. 5. Vibration spectra measured at $x_m = 0.28$, with the dash-dot line for uncontrolled case; the gray solid line for case 1 and the black solid line for case 2.

might be an excessive goal for a single actuator to damp five modes simultaneously. This prompts a second test as explained in the next subsection.

4.3. Case 2: damping three modes

In this case, the controller is designed to only damp the first three modes. A first order actuator filter $F_a(s) = (s + 15)^{-1}$ is included in the TFM and tested here. This is equivalent to adding $(s + 15)$ to the denominator of $\boldsymbol{T}(s)$. In general, one may simulate more complicated actuator/sensor filters by adding the filter numerators and denominators to the numerator and denominator of TFM, respectively. In reality, however, the actuator/sensor dynamics are automatically included in the TFM during the identification process for $\boldsymbol{T}(s)$.

Obviously, the effect of $F_a(s)$ is not the removal of the fourth and fifth modes from the model as assumed by simple mode truncation. Since the resonant frequencies of these modes are $\omega_4 = 24.18$ rad/s and $\omega_5 = 39.97$ rad/s, $F_a(s)$ introduces distortions to all modes. Inclusion of actuator/sensor filters is analytically more accurate to mode truncation, and not too complicated as demonstrated by this example.

The objective of damping the first three modes is prescribed to the controller via a new prototype polynomial $p(s) = (s + 12)\prod_{k=1}^{3}(s^2 + 0.27\omega_k s + \omega_k^2)\prod_{k=4}^{5}(s^2 + \omega_k^2)$. One can see that the damping ratio for the first three modes has been increased, whereas damping ratio for the fourth and fifth modes remains uncontrolled. Coefficients of $p(s)$ are then substituted into Eq. (16) together with coefficients of $d(s)$ and $\boldsymbol{N}(s)$, so that the controller coefficients can be solved by a

routine inversion. Vibration spectra for case 2 are plotted in Figs. 2–5 as black solid lines. Since the actuator is required to damp fewer modes, it is able to introduce more damping without requiring an excessive high-gain.

4.4. Experimental verification

The proposed controller is applied to damp an acoustical field in a $15 \times 12 \times 200\,\text{cm}^3$ duct. The actuator is a speaker placed in the middle of the duct and two sensors are placed 20 cm away in each side of the speaker. Frequency response characteristics of the sensor and anti-alias filters are available as plots, but not as transfer functions. As a result, the transfer matrix has to be identified to include actuator/sensor dynamics. It is not necessary to separate the actuator/sensor dynamics from the acoustical path in the identification process.

The anti-alias filter has a cut-off frequency at 900 Hz as shown in Fig. 6. Theoretically, a truncated model for the system has an order of $m = 24$ since 12 resonant modes are inside the range of 0–900 Hz. Practically, however, the order of the model is 60 to include dynamic effects outside the range of 0–900 Hz. This is an important feature of the proposed method discussed in Section 2.1. The controller parameters are computed using the linear matrix inequality (LMI) toolbox of Matlab with an $\mathbf{H}_\infty$ constraint given by Eq. (21). The performance of the controller is plotted in Fig. 6 where the resonant peaks are well damped by the proposed controller.

Since an active controller can only damp a finite number of resonant peaks, there are always resonant peaks not damped by the controller. The proposed method has an advantage, because its

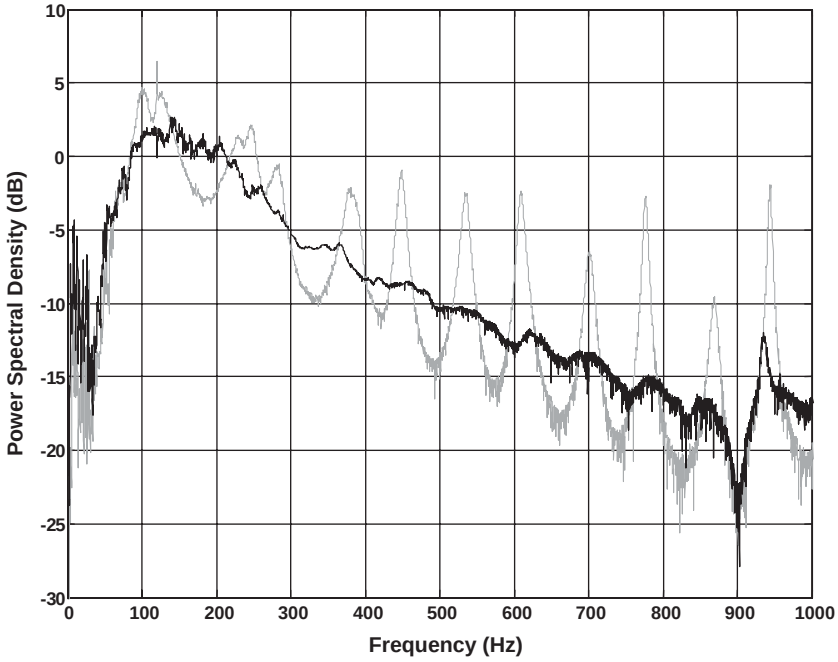

Fig. 6. Noise power spectrum densities, gray curve for uncontrolled noise; solid curve for actively damped noise.

controller is designed by taking the actuator/sensor dynamics into analytical account. The controller damps resonant peaks inside the pass-band of actuator/sensor dynamics very well without introducing any negative effects to other resonant peaks outside the pass-band of the actuator/sensor dynamics. This is verified in the experimental result of Fig. 6.

5. Conclusion

A robust controller is proposed for active damping of vibration fields. It is suitable for applications where model parameters, such as eigenfunctions or mass/stiffness coefficients of finite elements, are not analytically available or difficult to measure accurately. In these cases, one may apply an identification algorithm described in Ref. [12] to obtain the TFM model with identification errors bounded by small norms. The closed-loop stability margin of the proposed controller is analytically available by Eq. (21). The closed-loop eigenvalues of the vibration field can be placed inside a disk with radius $\gamma < 1$, in the presence of bounded identification errors. This is a feature not analytically available for other vibration controllers based on the modal or physical state-space models.

Acknowledgements

The work described in this paper was substantially supported by a grant from the Research Grants Council of the Hong Kong Special Administration Region (Project No. PolyU 5175/01E).

References

[1] L. Meirovitch, Dynamics and Control of Structures, Wiley, New York, 1990.
[2] J.S. Vipperman, R.L. Clark, Multivariable feedback active structural acoustic control using adaptive piezoelectric sensoriactuators, Journal of the Acoustical Society of America 105 (1) (1999) 219–225.
[3] N. Rizet, M. Brissaud, P. Gonnard, J.-C. Bera, M. Sunyach, Modal control of beam flexural vibration, Journal of the Acoustical Society of America 107 (4) (2000) 2061–2067.
[4] S. Griffin, C. Hansen, B. Cazzolato, Feedback control of structurally radiated sound into enclosed spaces using structural sensing, Journal of the Acoustical Society of America 106 (5) (1999) 2621–2628.
[5] H.T. Banks, Z-H. Luo, L.A. Bergman, D.J. Inman, On the existence of normal modes of damped discrete-continuous systems, American Society of Mechanical Engineers Transactions of Journal of Applied Mechanics 65 (1998) 980–989.
[6] K. Seto, M. Ren, F. Doi, Feedback vibration control of a flexible plate at audio frequencies by using a physical state-space approach, Journal of the Acoustical Society of America 103 (2) (1998) 924–934.
[7] K. Seto, M. Ren, F. Doi, Modeling and feedback structural acoustic control of a flexible plate, Transactions of the American Society of Mechanical Engineers Journal of Vibration Acoustics 123 (1) (2001) 18–23.
[8] T. Samejima, Modifying modal characteristics of sound fields by state feedback control, Journal of the Acoustical Society of America 110 (3) 1408–1414.
[9] K.Y. Lam, X.Q. Peng, G.R. Liu, J.N. Reddy, Finite element model for piezoelectric composite laminates, Smart Materials and Structures 6 (1997) 582–591.
[10] X.Q. Peng, K.Y. Lam, G.R. Liu, Active vibration control of composite beams with piezoelectrics: a finite element model with third-order theory, Journal of Sound and Vibration 209 (1998) 635–650.

[11] G.R. Liu, X.Q. Peng, K.Y. Lam, J. Tani, Vibration control simulation of laminated composite plates with integrated piezoelectrics, Journal of Sound and Vibration 220 (1999) 827–864.
[12] G.C. Goodwin, K.S. Sin, Adaptive Filtering Prediction and Control, Prentice-Hall, Englwood Cliffs NJ, 1984.
[13] K. Nassiri-Toussi, W. Ren, Indirect adaptive pole-placement control of MIMO stochastic systems: self-tuning results, IEEE Transactions on Automatic Control 42 (1) (1997) 38–52.
[14] M.T. Soylemez, N. Munro, Parametric solution to the pole assignment problem using dynamic output-feedback, IEEE Transactions on Automatic Control 46 (5) (2001) 711–723.
[15] D.J. Inman, Engineering Vibration, Prentice-Hall, Englewood Cliffs, NJ, 1994.